Geothermics 50 (2014) 91–100

Contents lists available at ScienceDirect

Geothermics

journal homepage: www.elsevier.com/locate/geothermics

Evaluating the Chingshui geothermal reservoir in northeast Taiwan with a 3D integrated geophysical visualization model

Ping-Yu Chang[a,*], Wei Lo[b], Seng-Rong Song[c], Kong-Ruei Ho[b], Chia-Shan Wu[a], Chow-Son Chen[d], Yu-Chi Lai[e], Huei-Fen Chen[a], Hseuh-Yu Lu[f]

[a] Institute of Applied Geosciences, National Taiwan Ocean University, Keelung 20224, Taiwan
[b] Department of Materials and Mineral Resources Engineering, National Taipei University of Technology, Taipei 10608, Taiwan
[c] Department of Geosciences, National Taiwan University, Taipei 10601, Taiwan
[d] Department of Geosciences, National Central University, Jongli, Taiwan
[e] Department of Informatics, National Taiwan University of Science and Technology, Taipei 10601, Taiwan
[f] Department of Earth and Environmental Science, National Chung Cheng University, Chia-Yi, Taiwan

ARTICLE INFO

Article history:
Received 26 November 2011
Accepted 18 September 2013
Available online 15 October 2013

Keywords:
Geothermal reservoir
Visualization model
Geophysics

ABSTRACT

In the current study, we assess the Chingshui geothermal reservoir with a three-dimensional visualization model that integrates geophysical measurements with well logs. To re-evaluate the geothermal reservoir quantitatively, we reprocessed resistivity measurements from a series of studies conducted nearly 40 years ago, as well as from the magnetotelluric (MT) explorations performed recently in the Chingshui area. We established a three-dimensional (3D) visualization model that integrates these different geophysical survey results as well as the well-logs to better perform the spatial relationships between them. From the orthogonal bipole–bipole resistivity surveys, we have identified several regional conductive structures with resistivity of less than 50 Ohm-m representing the major fault zones of the Dahsi, Xiaonanao, and Chingshuihsi faults. Among them, the Chingshui fault is located along the Chingshuihsi River valley and is associated with hot spring features. The collinear Schlumberger survey along the Chingshuichi Valley identified three relatively conductive regions with resistivity of less than 20 Ohm-m. The MT interpretation shows that the structure associated with the geothermal reservoir extends from these near-surface fractures to a depth of −1500 m toward the south in the fault zone. The identified production zone from the core drilling records is consistent with the conductive structure in the MT inverted image. In addition, the structure seems to consist of two sub-regions: a somewhat shallow one at a depth of between −400 and −800 m in the north and a somewhat deep one at a depth of between −600 and −1500 m in the south. From the 3D model, we estimate that the volume of the Chingshui geothermal reservoir is about 9.54×10^7 m^3. Given a gross porosity of 0.1 and 100% saturation for the fracture zones from the core logs, the inferred Chingshui geothermal reservoir contains about 10 million cubic meters of geothermal fluids.

1. Introduction

The Chingshui geothermal field is located in a 1.3-km^2 area, approximately 13 km southwest of Ilan City in Northeast Taiwan (Fig. 1). Hot springs were found along the Chingshuihsi River and pointed to the possibility that the area was a geothermal region. In the 1970s, the Industrial Technology Research Institute (ITRI) conducted a series of reconnaissance geophysical surveys, including surveys on gravity, electrical resistivity, and spontaneous potential (Lee, 1994), to locate potential drilling sites (Fig. 2). Following the ITRI surveys, Chinese Petroleum Company (CPC) drilled 19 probing wells in the area and later completed seven production wells for power generation (Tong et al., 2008). In 1981, Taiwan's National Science Council funded the construction of a power plant with 3-MW power-generation capacityin Chingshui, Ilan and the power plant was hand over to the Taipower Company for operation. The plant was ceased to function in 1993 owing to scaling problems and decreased fluid production.

In 2008, the Taiwan Government initiated a new campaign for geothermal exploration in the Chingshui area owing to Taiwan's growing need for clean energy. Tong et al. (2008) pointed out that although a few exploration surveys had been conducted the reservoir of the Chingshui geothermal field had yet to be clearly delineated (e.g., Hsiao and Chiang, 1979; Lee, 1994; Su, 1978; Tong

* Corresponding author at: Institute of Applied Geosciences, National Taiwan Ocean University, No. 2, Beining Road, Keelung City 20224, Taiwan.
Tel.: +886 2 24622152x6510.
E-mail addresses: pingyuc@mail.ntou.edu.tw, pingyuc@gmail.com (P.-Y. Chang).

0375-6505/$ – see front matter © 2013 Elsevier Ltd. All rights reserved.
http://dx.doi.org/10.1016/j.geothermics.2013.09.014

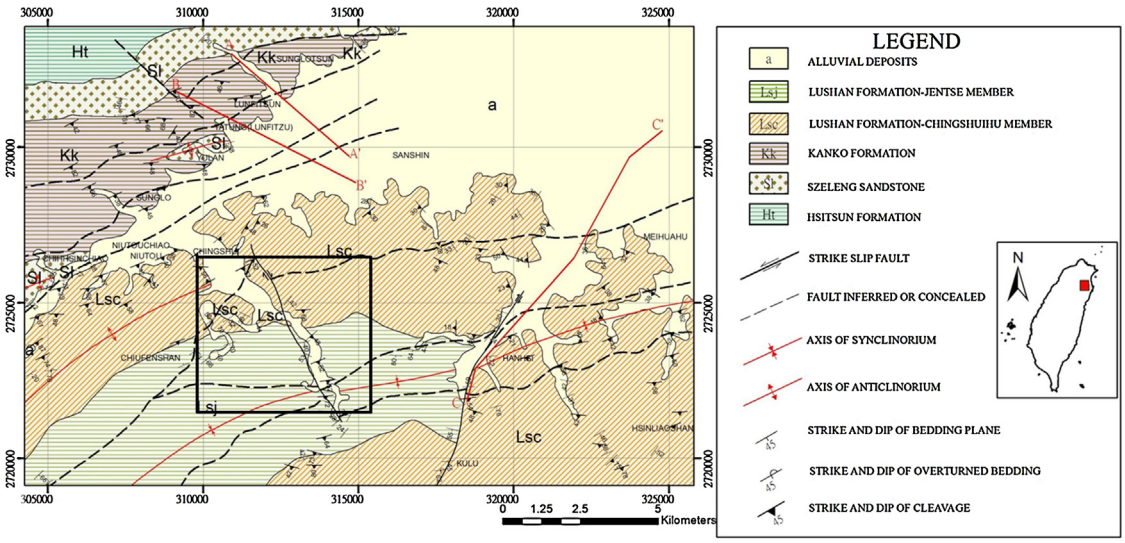

Fig. 1. The regional geology map of the study area; modified from Tseng (1978) and Lin and Lin (1995). The square area indicates the geophysical survey region for the Chingshui geothermal field.

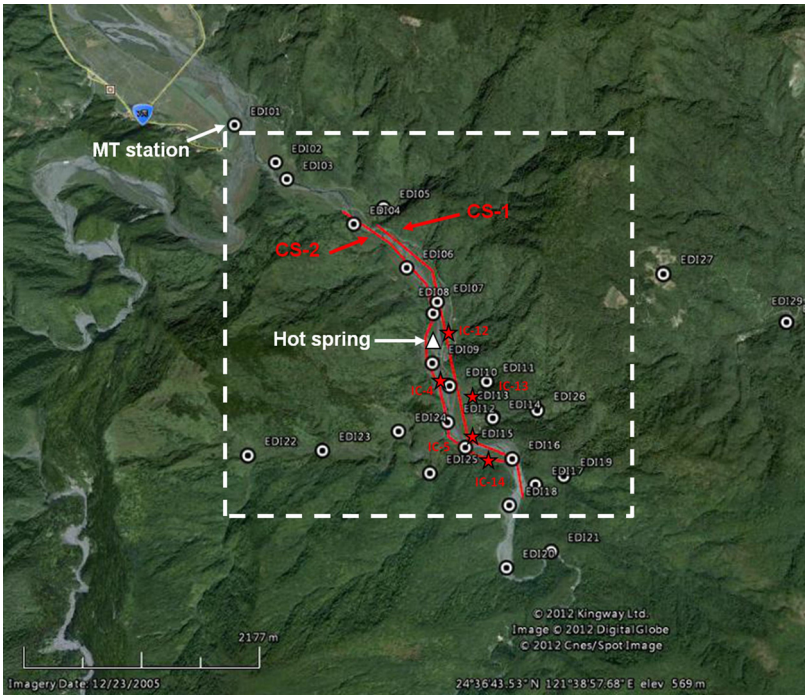

Fig. 2. The satellite image showing the enlarged square area in Fig. 1 and the locations of the hot spring outcrop (the red triangle), the electrical resistivity surveys along the Chingshui river (the two red lines), production wells (the red stars), and the MT stations (the small white circles). Dashed-line square indicates the area of the 3D visualization model shown in Fig. 7. (For interpretation of the references to color in this figure legend, the reader is referred to the web version of this article.)

et al., 2008; Tseng, 1978). The team collected data from gravity, magnetic, and MT measurements and tried to interpret the structure of geothermal reservoirs (Tong et al., 2008). They relied mainly on the MT inversion results to delineate the geothermal reservoir structures because the magnetic and gravity data could not provide as good a resolution as the EM and resistivity measurements. However, the locations of surface hot springs are inconsistent with the locations of low resistivity regions in MT inverted images. Neither the fracture zones nor their orientations, as indicated in well logs, can be well correlated to the low resistivity regions in the MT inverted images. The inconsistency raises questions about the appropriateness of the MT inverted images, leaving the reservoir structures in the Chingshui area an unknown variable.

In this study, we have tried to review and reprocess the resistivity and MT measurements with new processing and inversion strategies. The electrical resistivity data derive from surveys conducted by ITRI from 1973 to 1975 (Lee, 1994). These resistivity surveys feature two configurations: the orthogonal bipole–bipole method and the collinear Schlumberger method. The ITRI team used the orthogonal bipole–bipole method while fixing both transmitter and receiver dipole lengths at 500-m. The receiver dipole was moved across the Chingshui area while the dipole direction was kept normal in relation to the source dipole. The collinear Schlumberger method was utilized along the two sides of the Chingshuihsi River. The MT raw data were the same as those in Tong et al. (2008) and were reprocessed with both one- and two-dimensional

inversion methods and different processing strategies. We then compared the inverted resistivity data with the CPC records of core logs to verify the resulting images and to settle upon an interpretation for the geothermal reservoir. For the purpose of the current study, we have constructed a three-dimensional visualization model that integrates these geophysical measurements and well logs to show the spatial connections of the geophysical features in a 3D framework.

2. Geological setting

The Ilan Plain is thought to have taken shape from the extension of the Okinawa Trough back arc basin within the Eurasian continental lithosphere (Lai et al., 2009). The recent extension of the Okinawa Trough by approximately 0.1 Ma involved ENE- and WSW-trending normal faults dipping toward the Okinawa Trough axis with offsets from a few meters to tens of meters (Lai et al., 2009; Sibuet et al., 1998) in the westernmost part of the trough. Unconsolidated alluvial deposits from the Lanyanghsi River were laid over the rock basement exhibiting the normal faults. Chiang (1976) and Hsu et al. (1996) have identified both ENE faults and WSW faults beneath the unconsolidated deposits by means of seismic reflection and refraction profiles across the Ilan Plain and by means of magnetic-anomaly analyses. These ENE faults and WSW faults seem to be in the prolongation of thrust faults found around the Ilan Plain (Benoit Deffontaines et al., 2001). The Lishan Fault separates the Hsuehshan terrain from the Central Ranges and has previously been interpreted as a normal fault (Lee et al., 1997). The fault separates the Oligocene sandstone and the slate of the Hsuehshan terrain on the west side from the Miocene slate of the Central Ranges on the east side (Fig. 1). The Chingshui-Sanshin-Hanhsi area, consisting of Taiwan's largest existing productive geothermal field in Chingshui (Lee, 1994), is located at the northeastern end of the sub-metamorphic zone of Taiwan. The rocks hosting the geothermal field are likely to be of prehnite–pumpellyite metamorphic facies.

As shown in Fig. 1, the rocks cropping out in the mapped area can be divided into three formations: The Lushan Formation of the Miocene Age, which can be divided into two members: the Chingshuihu member and the Jentse member, the Kanko Formation, Szeleng Sandstone, and the Hsitsun Formation. The Chingshuihu member is composed of slate or phyllite with thin beds of meta-sandstone, and the Jentse member is alternation of argillite or meta-sandstone. The Kanko Formation is conformably overlaid by the Chingshuihu member. It is composed chiefly of slate, occasionally intercalated by thin beds of fine-grained sandstone. The Szeleng Sandstone is composed mainly of thick-bedded, gray-to-grayish-white, medium-to-coarse-grained quartz meta-sandstone. The Hsitsun Formation consists mainly of alternations of silty argillite and fine-grained meta-sandstone, thick bedded argillite or slate with thin bedded meta-sandstone intercalation (Lin and Lin, 1995).

The Lushan Formation constitutes a synclinorium according to the vergence and sense of rotation in minor folds. The synclinorium axis is located at the upstream region of the Chingshuihsi River within the Jentse member. The dip of the fold plane is steep to the southeast and the strike of the fold plane is parallel to the Chihlukeng River. The Chingshuihsi fault is a right-lateral fault and is sub-parallel to the Chingshuihsi River. Upstream of the Chingshuihsi River, the Xiaonanao fault is cut by Chingshuihsi fault. Lin and Lin (1995) proposed that the Chingshui geothermal field might be related to the fracture zone of the Chingshuihsi fault (Tong et al., 2008). The Xiaonanao fault is a normal fault and dips 60–70° to the south. Many landslides have occurred along the Chihlukeng River by the Xiaonanao fault. The Dahsi fault is located downstream of the Chingshuihsi River and across the Dahsi River. There are a series of normal faults that have a north-eastern extension distributed in the Chingshui-Sansin-Hanchi area. Most of them dip to the east, but two of them dip to the west with an angle of 60–70° and are distributed along the Dahsi River.

3. Data processing and inversion

3.1. Resistivity surveys

The resistivity surveys in Chingshui area were accomplished with the orthogonal bipole–bipole method and the collinear Schlumberger method by the ITRI team. The team carried out the orthogonal bipole–bipole surveys by fixing the transmitter dipole at one position and moving the receiver dipole with the same separation length in the perpendicular direction across the survey area including the Chingshuihsi River valley. Both the transmitter and receiver dipole lengths were kept at 500 m. Four groups of apparent resistivity datasets, i.e., four datasets with different fixed transmitter positions, were collected with four individual transmitter locations. The approach resulted in nearly complete data coverage within the area highlighted by the dashed white line on Fig. 2.

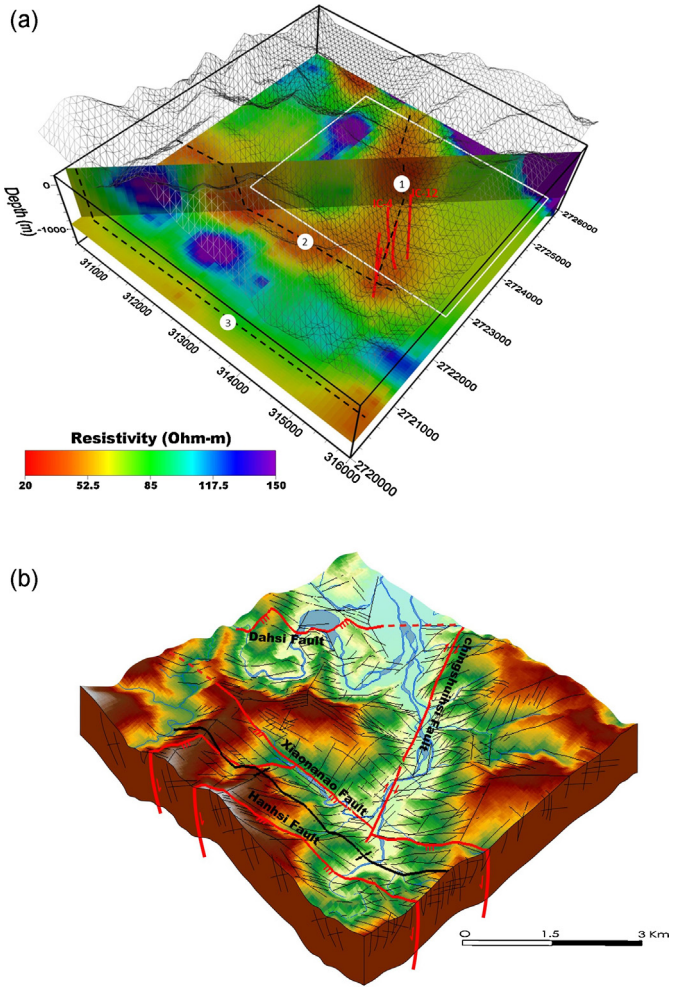

Fig. 3. (a) The inverted orthogonal bipole–bipole images of the study area shown in Fig. 2. The dashed lines 1, 2, and 3 represent the conductive structures along the Chingshuihsi fault, the Xiaonanao fault, and the Hanhsi fault, respectively. The white square mark the 3D visualization model area indicated in Fig. 2, and the red vertical lines denotes the production wells. (b) The sketch of regional fractures and faults from the geology field surveys.

In addition, the same team also collected the collinear Schlumberger measurements by increasing the distance between the two transmitter electrodes while fixing the central point of the receiver potential electrodes for depth sounding. The transmitter dipole lengths were increased from 300 m to 1300 m, and the potential dipole lengths were increased from 60 m to 260 m. The ratio of the current to the potential dipole lengths was kept at 5–1 during the depth sounding. Then the receiver electrodes were moved 100 m laterally to a new position for another depth sounding, and the measurements were calculated by means of repeating the same process along the survey line. The measured data were then calculated into apparent resistivity, and were plotted according to the electrode positions and dipole separations to form a pseudo-section. Because the ITRI plotted and kept the data records only in pseudo-sections, we had to digitize them in order to use the data for building the resistivity model with the inversion code. Pseudo-sections were scanned, and data were then read manually according to the contour plot. Because the old records were not plotted on the UTM map, we transformed the contour plots into transparent slides and overlapped onto a UTM map in order to locate the survey lines in the current UTM system. Lastly we performed QA/QC by comparing the calculated digitized apparent resistivity values with the pseudo-section contour plots in the old records.

The Schlumberger and orthogonal bipole–bipole resistivity data were inverted with EarthImager^{TM} 2D and EarthImager^{TM} 3D software (AGI, 2008, 2009), respectively. Both EarthImager^{TM} 2D and EarthImager^{TM} 3D use a forward-modeling subroutine and nonlinear optimization technique to calculate resistivity values. AGI (2009) implemented Dirichlet and mixed boundary conditions (Dey and Morrison, 1979) in the EarthImager^{TM} program. The matrix system was iteratively solved according to a conjugate gradient method.

3.2. MT data processing

We adopted the same data from the MT measurements collected by ITRI (Tong et al., 2008). In contrast to the approaches used in Tong et al. (2008), we reviewed the MT spectrums and

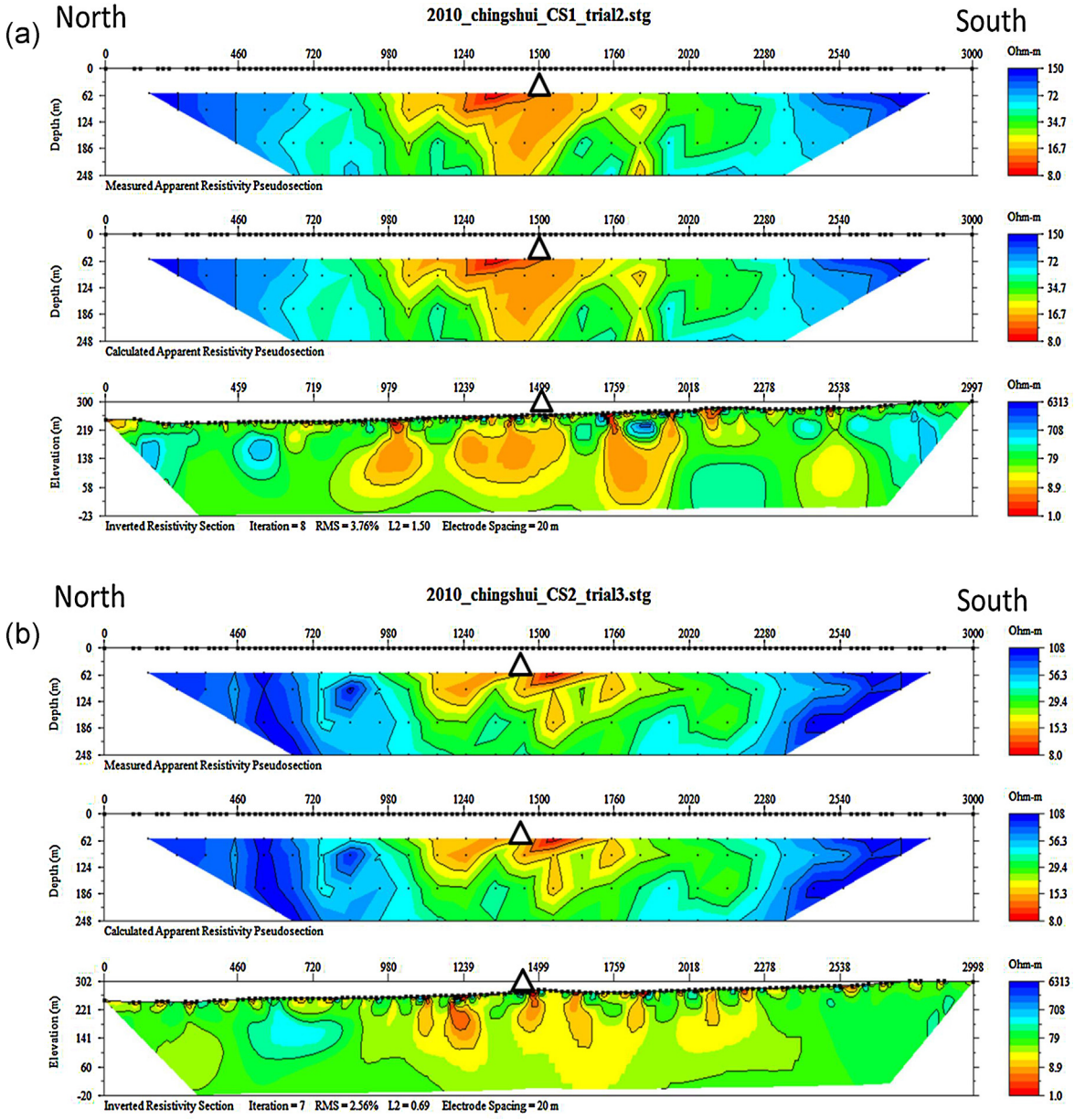

Fig. 4. From top-to-bottom: the measured pseudo-section, the estimated pseudo-section, and the inverted results of the (a) CS-1 and (b) CS-2 profiles conducted along the Chingshuihsi river. Overturned triangles show the projected location of the hot spring in the Chingshuihsi valley.

found the measurements at low frequencies exhibited high variation errors. Hence, we used a high-pass filter of 0.5 Hz to select the audio magnetotelluric (AMT) data from the MT measurements. Given a rough estimation of 20–500 Ohm-m for regional rock bulk resistivity measured by Tong et al. (2008), we worked with a skin depth ranging from 2000 m to 15,000 m for the MT exploration. The MT data were corrected for static shift with the low pass spatial method (Sternberg et al., 1982, 1988). We decided the area-average of the apparent resistivity sounding by selecting the sites with least difference between the apparent resistivity and phase curves. Individual apparent resistivity curves were then shifted with respect to the area-average. To invert the AMT data, we then used the 1D inversion code, the IPI2Win (MT), provided by Bobachev (2003) at Moscow State University. The data inversions involved TM, TE modes separately. The IPI2Win uses an iterative regression method to address both the apparent resistivity and the phases of the MT measurements. In the current study, ten MT stations along the Chingshuihsi River were selected for the 1D inversion in the north–south direction, and six MT stations were chosen for the 1D inversion in the east–west direction. To maintain the consistency of the inversion process, we first inverted the data from a starting station with a uniform resistivity model. Then we used the inverted results as the initial model for inverting the resistivity model of the neighboring station. Finally, the inverted results of all stations were stitched together to perform the "stitched cross-sections" of resistivity.

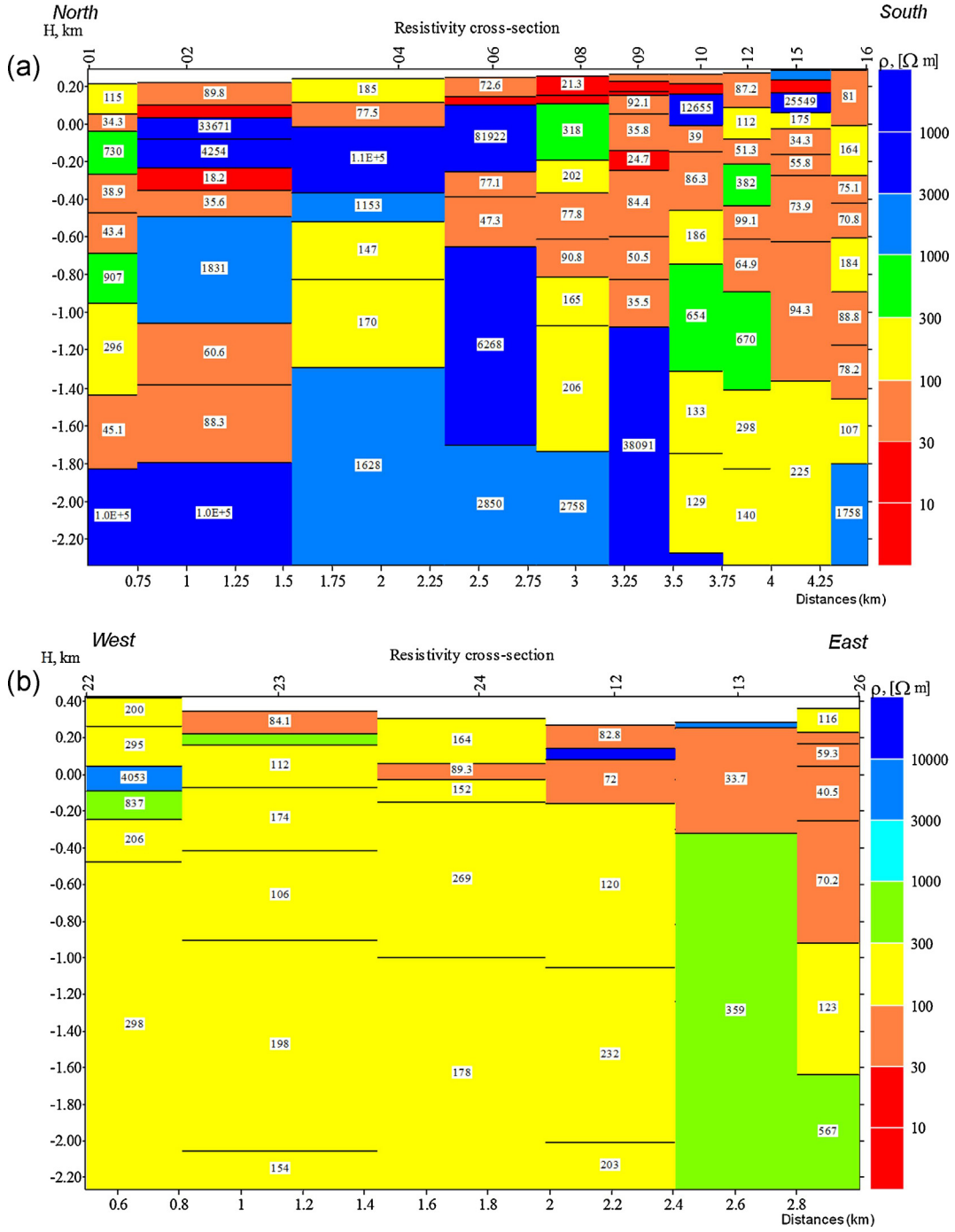

Fig. 5. (a) The stitched 1D MT inverted result of stations in the north–south direction. (b) The stitched 1D MT inverted result of stations in the east–west direction.

In addition to the 1D inversion, we performed a 2D inversion with Occam's inversion code, OCCAM2DMT V3.0. The inversion code is an implementation of the general Occam procedure of Constable et al. (1987) and was extended to two dimensions by de Groot-Hedlin and Constable (1990). We carried out the 2D MT forward calculations with code provided by Wannamaker et al. (1987) using reciprocity to calculate the Jacobian (Pastana de Lugão and Wannamaker, 1996). In the current study, thirteen MT stations along the Chingshuihsi River were selected for the 2D inversion in the north–south direction, and six MT stations were chosen for the 2D inversion in the east–west direction. For each station, we selected the measurements at 38 different frequencies ranging from 0.1 Hz to 320 Hz.

4. Results

4.1. The orthogonal bipole–bipole surveys

Fig. 3a shows the inverted results from the orthogonal bipole–bipole resistivity surveys. The measurements were inverted with the 3D inversion code, EarthImager3D. The 3D inversion achieved its optimal solution with an RMS of 16% after 8 iterations. The surveys were conducted mainly in the Chingshui area. In Fig. 3a, we present the bipole–bipole results with a vertical resistivity cross-section along the northeast–southwest direction, and a horizontal slice at a depth of −800 m from the ground surface. Fig. 3b shows the interpretation of regional fractures and fault

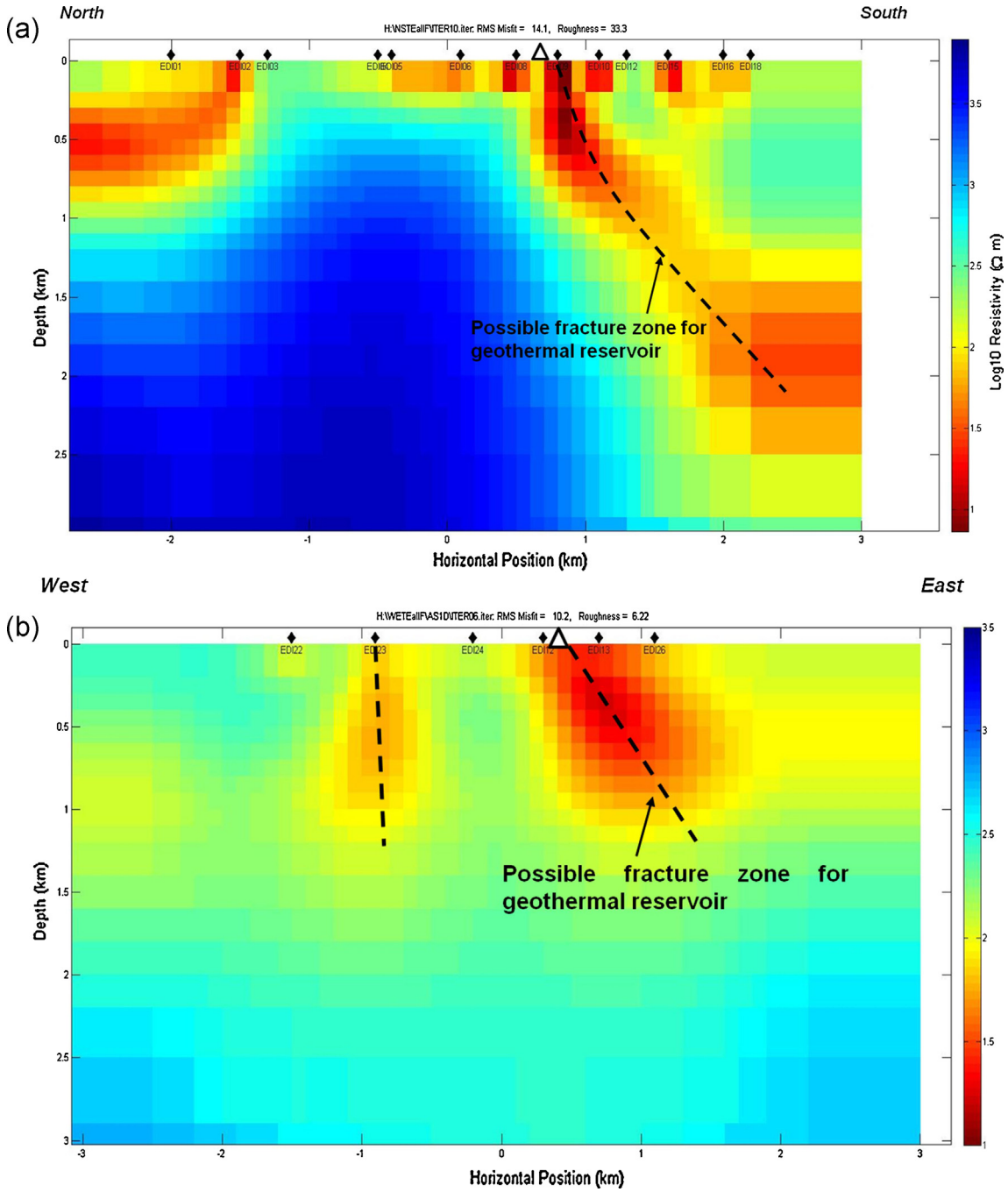

Fig. 6. (a) The 2D MT inversion result of stations in the north–south direction. (b) The 2D MT inversion result of stations in the east–west direction. White triangle shows the projected location of hot spring in the Chinshuihsi valley.

structures based on the measurements of fracture orientation and geology field surveys. We use tomography to confirm the existence of the faults (as shown in Fig. 3b) identified with field geology surveys in the fractured slates. From the bipole–bipole resistivity survey, we found three very conductive structures with resistivity of less than 50 Ohm-m, as shown in Fig. 3a. Structure 1 is located roughly along the Chingshuihsi River in the north–south direction and likely represents the Chingshuihsi fault, as shown in Fig. 3b. Structure 2 seems to be the boundary that separates the two resistive regions and has a similar E–W direction to the Xiaonanao fault. Structure 3 is orientated in the E–W direction in the southern part of the survey area. Compared with Fig. 3b, structure 3 is likely the Hanhsi fault. The hot springs in the Chingshui area are located in the junction area of the Chinshuihsi fault and the Xiaonanao fault. This junction area is associated with the hot springs, and features the potential fractural geothermal reservoir in the area.

4.2. The collinear Schlumberger surveys

Fig. 4a and b shows the inverted resistivity image of CS-1 and CS-2 profiles, respectively. The two profiles were conducted at different sides along the Chingshuihsi River and the Chingshuihsi fault. Both CS-1 and CS-2 measurements were inverted with the 2D code, EarthImager 2D from AGI (AGI, 2009). In Fig. 4, the location of the hot spring appears near the IC-4 well on the images. The images show that the wall rock is relatively resistive and has a resistivity of over 80–100 Ohm-m. We found that three major conductive regions with resistivity of less than 20 Ohm-m are located from the ground surface to a depth of over 150 m in both the CS-1 and CS-2 resistivity images. The location of the middle conductive region is consistent with the hot spring. Hence, we have concluded that the conductive structures with very low resistivity are most likely the near-surface fractures filled with geothermal fluids. Unfortunately, the configurations of the Schlumberger surveys in this study can resolve only the near-surface structures, which are within 200–300 m of the surface. The configurations do not have enough resolution for deeper structures under the conductive structures. Therefore we need to use other geophysical data for better understanding the subsurface structures related to the geothermal fluid conduits.

4.3. The 1D MT inversion

MT data can be separated into transverse electric (TE) and transverse magnetic (TM) modes based on the orientation of the electric- and magnetic-filed to the regional dominant geological structures in the E–W direction as shown in Fig. 1. In the study both TM- and TE-mode data were inverted with IPI2Win (MT), respectively. Fig. 5a and b shows the inverted "stitched" images of 1D MT surveys in TM mode in the north–south and in TE mode in the east–west directions, respectively, since they perform the best contrast across the geothermal structures in the Chingshuihsi Valley. In Fig. 5a, a major conductive region with resistivity of less than 100 Ohm-m can be identified at a depth above −1200 m between MT Station 6 and Station 15. Despite the conductive regions near the surface, the conductive structure seems to dip toward the south with an angle of 60–65° on the stitched plane. One should note that the angle shown on the stitched plane is not the true dip and is presented here only for a reference. The near-surface conductive structure is likely the response from the saturated river bed, because the MT stations were installed roughly in the N–S direction along the Chingshuihsi river. The image also shows that the most conductive part of the region was located between stations 08 and 10 near the surface, because the area comprises the locations of hot springs in the Chingshuihsi river valley. In addition, a deeper conductive region with resistivity of less than 100 Ohm-m is parallel to the aforementioned conductive region at a depth of between −400 and −1100 m between stations 6 and 9. Because of its similar orientation to the major conductive structure, we have concluded that the conductive structure is a part of a major structure that is separated by the wall rocks. The inverted 1D MT image is shown in Fig. 5b. We identified two conductive regions corresponding to Fig. 5b: the one located under MT stations 12, 13, and 26, and the other one under station 23. The former conductive region under the MT stations 12,

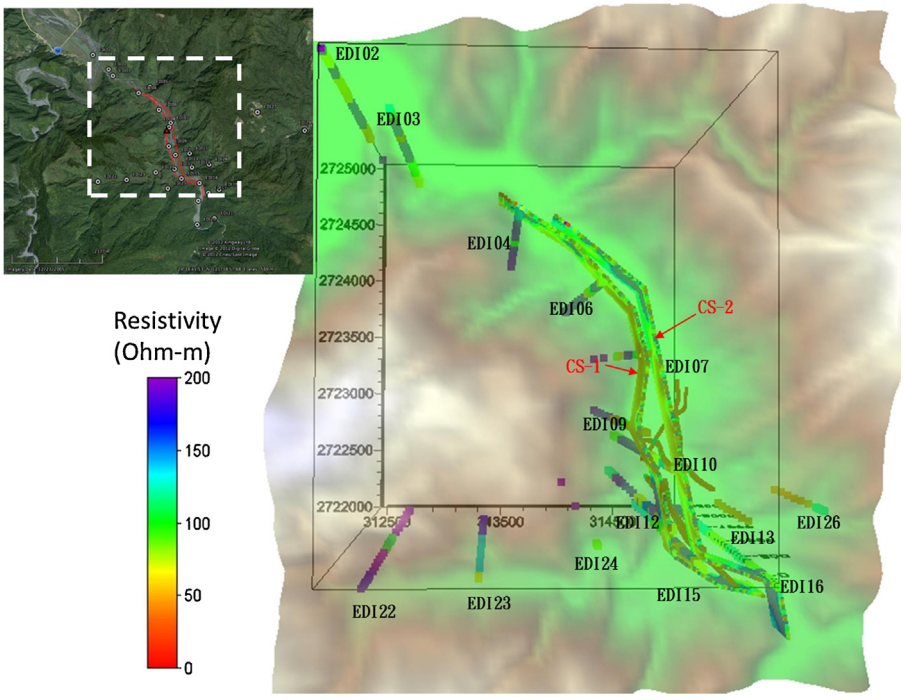

Fig. 7. The framework of the 3D geophysical visualization model of the Chingshui area with DTM topography. Vertical columns show the 1D inverted results from the MT measurements. CS-1 and CS-2 are the inverted results of the collinear Schlumberger surveys shown in Fig. 4.

13, and 26 coincides with the conductive structure identified from the N–S 1D MT image, and suggests that it is a part of the major structure related to the geothermal reservoir.

4.4. The 2D MT inverted images

For 2D MT inversion, we have tried to invert the data in TE, TM, and TE+TM modes and found that the TM mode shows a good agreement with the regional geological structures. Fig. 6 shows the inverted 2D MT images in the TM mode. In Fig. 6a, we found that a distinctive conductive structure with resistivity of less than 100 Ohm-m is located at the ground surface at the hot spring. The conductive structure dips toward the south at an angle of 55–65° on the projected N–S plane. The angle presented here is an estimation of the apparent dip on the N–S plane. It implies that the structure may have a true dip higher than 55–65°. The conductive structure found in the 2D MT-inverted image is consistent with the findings from the 1D stitched MT images and exhibits a similar dipping angle. This similar conductive structure may indicate the possible fracture zones filled with hot fluids for the geothermal reservoir. The 2D MT image in Fig. 6a seems to provide a better resolution for the conductive structure than the 1D MT images. In addition, in Fig. 6a, a shallow conductive structure is located at the ground surface at MT station 2 and dips toward the north at an angle of 40–45°. The influence of the saturated riverbed sediment was also noted near the ground surface in the 2D MT image in Fig. 6a.

The inverted 2D MT image in Fig. 6b is similar to the 1D MT image in the E–W direction. Two conductive structures with resistivity of less than 100 Ohm-m can be identified in Fig. 6b. The conductive structure under MT stations 12, 13, and 26 dips toward the east at an angle of 50–55° on the projected E–W plane. The conductive structure under station 23 is a vertical structure. The two conductive

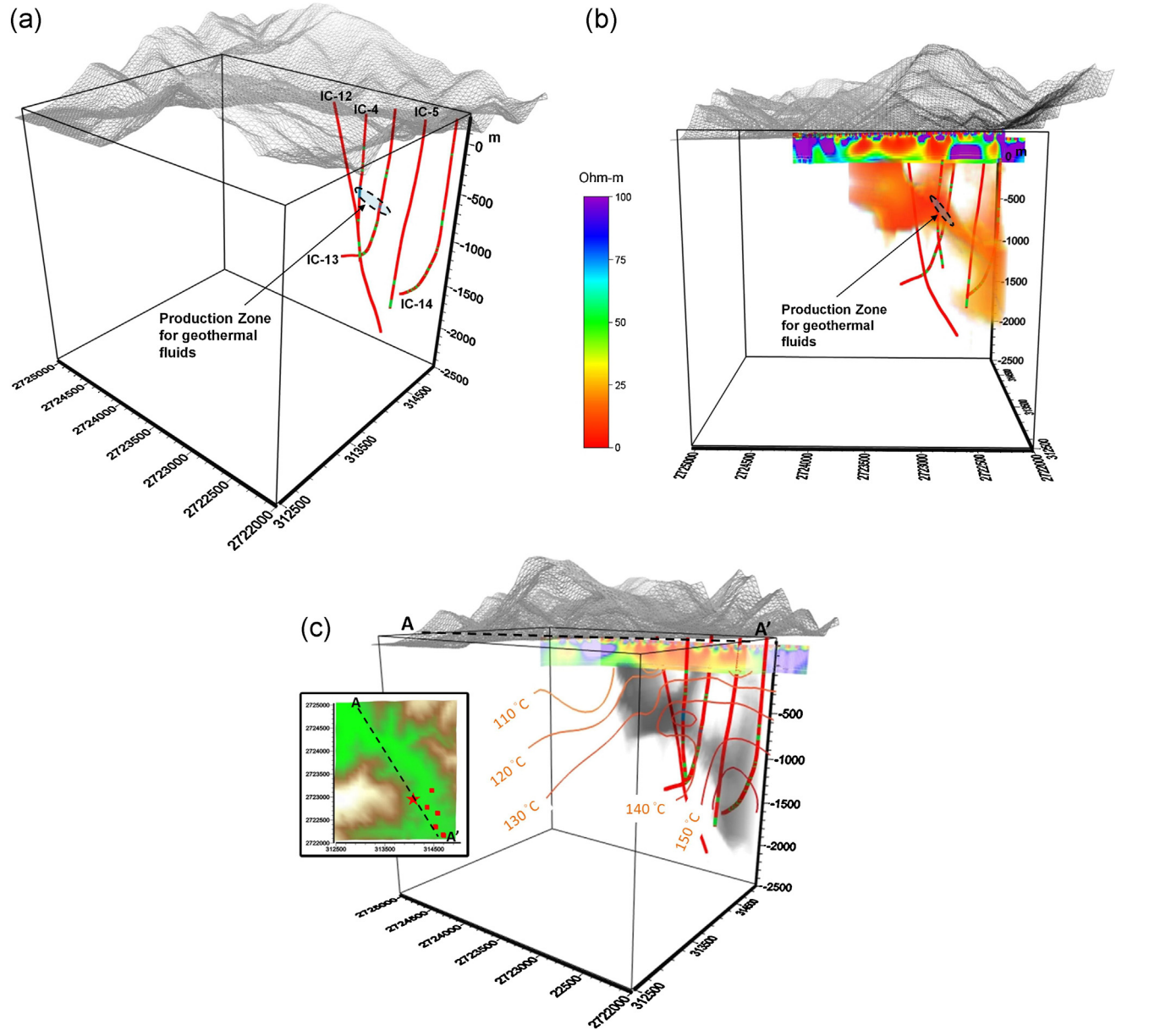

Fig. 8. (a) The geothermal wells in the Chingshui area. Fracture zones and production zones in the wells from well logs are indicated with green and blue colors, respectively. (b) The Oblique view of the 3D model showing the collinear Schlumberger survey results and the conductive region (resistivity <100 Ohm-m) from the MT surveys. (c) A side view of the 3D model with projected isotherms (solid lines) from the well logs on the cross section of A–A′ along the Chingshuihsi river, and the conductive region (the gray shadow area) from the MT surveys. (For interpretation of the references to color in this figure legend, the reader is referred to the web version of this article.)

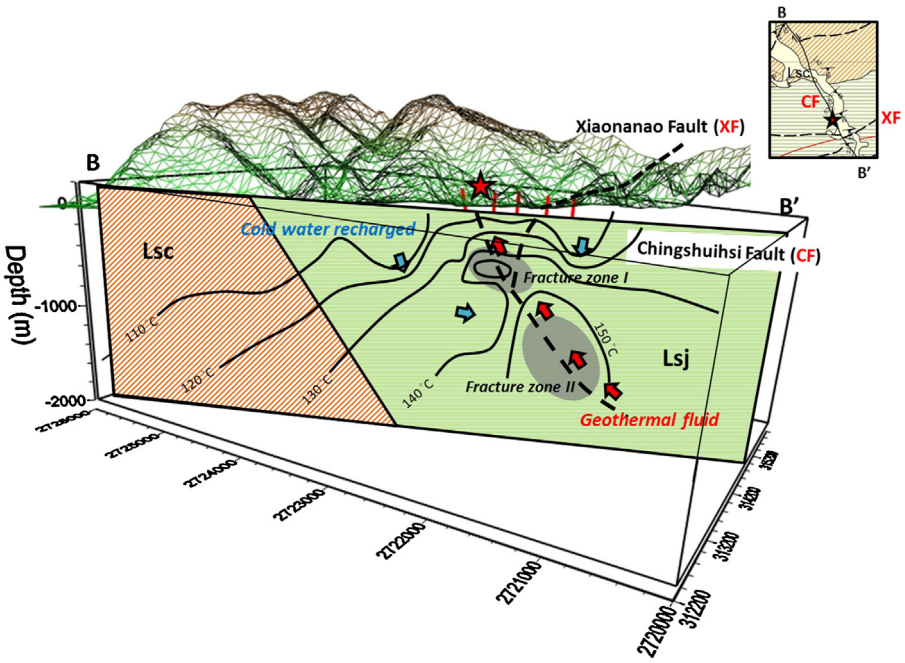

Fig. 9. The schematic diagram showing the forming mechanism of the Chingshui geothermal reservoir. Cold water may take the paths through the fracture openings to a greater depth along the Chinshuishi fault zone (B–B′). Due to the greater geothermal gradient in the Chingshui area, the fluid is gradually heated to over 200 °C along its flow paths. And the heated fluid goes through the south-dipping fracture structure illustrated in Fig. 8 to flow back to the surface outcrops. (Red star: the hot spring location, vertical red lines: well heads of the production wells, Lsc and Lsj: Chingshuihu member and Jentse member of the Lushan formation, respectively.) (For interpretation of the references to color in this figure legend, the reader is referred to the web version of this article.)

structures terminate at a depth of −1000 m and show no continuous tail below this depth. The findings suggest that the E–W plane obliquely intersects the main structure, whose orientation is mainly in the N–S direction.

5. Discussion

In the previous section, we present the results and interpretations from different geophysical surveys performed in the Chingshui area over the past few decades. These collected measurements differ from one another regarding spatial coverage and resolution, and therefore, the ITRI has interpreted these measurements individually in the past. To better correlate different geophysical measurements with the core logs, we construct a visualized model (Fig. 7) for illustrating the geophysical results and core logs in a 3D sense. Fig. 7 shows the plan view of the model range. All resistivity data and MT inverted results can be shown at once in the 3D model.We incorporated a digital terrain model (DTM) of the Chingshui area into the model to show the precise location of the geophysical features. Fig. 8a presents the locations and orientation of the geothermal wells in the area. Core logs as well as the well-logging measurements were digitized into the model database. From the core logs and well-logging measurements, we recorded the fracture zones and the production zones where geothermal fluids feeding in the database. Fig. 8a shows the fracture zones in green sectors and the production zones in blue sectors, respectively. A production/feeding zone dipping toward the South can be identified from records of well IC-4 and well IC-13.

Although the 2D MT images have better resolution for the conductive structure related to the geothermal reservoir than the 1D MT images, it is difficult to use the 2D MT images for estimating the volume of the geothermal reservoir. The 2D MT images are obtained by projecting measurements of different stations onto a plane and by inverting the measurements in a 2D sense. Hence, we use the 1D MT data, since they are similar to the 2D inverted results, and we interpolate the 1D MT data according to the inverse distance method for rendering a 3D MT resistivity model (Fig. 8b and c). From the 3D MT resistivity model, we isolate the conductive structures with resistivity of less than 100 Ohm-m under the region near the hot springs, as shown in Fig. 8b and c. Fig. 8c shows the projected static temperature contours from the CPC probing wells (measured while the wells were shut-off) and the MT conductive zone on the same vertical plane along the Chingshuihsi river. The conductive structure is consistent with the fracture zones and the high temperature areas (>140 °C) indicated in the core logs. In addition, the structure seems to consist of two sub-regions: a somewhat shallow one at a depth of between −400 and −800 m in the north and a somewhat deep one at a depth of between −600 and −1500 m in the south. The two sub-regions are connected together, and the connecting part coincides with the production zone indicated from the core log data. The shallower conductive sub-region has several vertical structures that extend upward to the ground surface. The vertical conductive structures are consistent with the conductive zones shown in the 2D dipole–dipole resistivity images and the hot springs. Disturbing of isotherms in Fig. 8c suggests that the surface cold water may recharge through some fractures in the Chingshuihsi fault zone. The agreement between the geophysical findings and the core log data suggests that the conductive volume may represent the potential geothermal reservoir. We estimate the volume occupied by the isolated regions with resistivity of less than 100 Ohm-m, and we conclude that the potential geothermal reservoir has a total volume of 9.54×10^7 m^3. From the geophysical results and the 3D model, we have illustrated the geothermal mechanisms in the Chingshui area. Although the heat sources remain unidentified, we now can declare that the geothermal fluid reservoir is located near the junction of the Xiaonanao fault in the Chingshuihsi fault zone (Fig. 9). The reservoir is constituted by a dominant fracture that is cropped out near the surface hot spring and dips toward the south to a depth of −1500 m in the Jentse member of the Lushan formation. Two larger fracture

zones can be found in the dominant fracture at a depth between −400 and −800 m, and between −600 and −1500 m, respectively. From the production test records the temperatures in some production wells can be gradually raised from their static temperatures up to over 200 °C during the flowing test. The facts imply that a recharge of colder water may take along routes through fractures in the Chingshuihsi fault zone and gradually heat up to over 200 °C due to the high geothermal gradient in the area. Hot fluid then takes a shorter path to flow through the reservoir and mixes with shallow cold groundwater until reaching the ground surface, as shown in Fig. 9.

6. Conclusions

We have reprocessed and inverted resistivity measurements from a series of surveys conducted nearly 40 years ago, as well as from the magnetotelluric (MT) explorations performed recently in the Chingshui area, to reevaluate the potential of the geothermal reservoir quantitatively. We used the results from the resistivity and MT surveys, as well as the well logs, to construct a 3D visualization model for assessing the geothermal potential of the Chingshui area. Although the geophysical surveys employed different geophysical methods and therefore provide different physical measures, the integrated 3D visualization images show a consistent spatial distribution of anomalous regions in different measurements. The model helps us to review the geothermal reservoir quantitatively in a 3D sense. From the orthogonal bipole–bipole resistivity surveys, we have identified several regional conductive structures with resistivity of less than 50 Ohm-m in the Chingshui area. These conductive structures are consistent with the geological findings in the area and, thus, represent the major fault zones of the Dahsi, Xiaonanao, and Chingshuihsi faults. Among the regional faults, the Chingshuihsi fault is located along the Chingshuihsi River valley. We identified three relatively conductive regions with resistivity of less than 20 Ohm-m on the basis of the collinear Schlumberger survey along the Chingshuihsi river. These very conductive regions show the responses from the fractures associated with the near surface geothermal fluid conduits in the Chingshuihsi fault zone. In addition, the MT interpretation from both the 1D and 2D inversions show that the conductive structure with resistivity of less than 100 Ohm-m extends from these near-surface fractures to a depth of −1500 m toward the south in the fault zone. The identified production zone from the core drilling records is consistent with the conductive structure in the MT inverted image. Therefore, we conclude that we have imaged the geothermal structure that is dipping toward the south in the Chingshuihsi fault zone. We estimated the volume occupied by the regions with resistivity of less than 100 Ohm-m, and conclude that the potential geothermal reservoir has a total volume of 9.54×10^7 m^3. Given a gross porosity of 0.1 and 100% saturation for the fracture zones from the core logs, we estimate that the Chingshui geothermal reservoir contains about 10 million cubic meters of geothermal fluids. And the planning reinjection should focus on the southern part of the Chingshuihsi valley for better heat-exchange efficiency.

Acknowledgements

The study is funded by the National Science Council under the project grant NSC98-3114-M-002-001 and NSC99-3114-M-002-001. We are grateful to Dr. Constable at the Scripps Institution of Oceanography and Bobachev at Moscow state University for providing MT inversion codes, and with deepest appreciation to CPC and ITRI in Taiwan for provide valuable raw data for study.

References

AGI, 2008. Instruction Manual for EarthImager 3D version 1.5.3. Advanced Geosciences, Inc., Austin, TX.
AGI, 2009. Instruction Manual for EarthImager 2D version 2.4.0. Advanced Geosciences, Inc., Austin, TX.
Benoit Deffontaines, C.S.L., Angelier, J., Lee, C.T., Sibuet, J.C., Tsai, Y.B., Lailemand, S., Lu, C.Y., Lee, C.S., Hsu, S.K., Chu, H.T., 2001. Preliminary neotectonic map of onshore-offshore Taiwan. Terrestrial, Atmospheric and Oceanic Sciences, 339–349.
Bobachev, A., 2003. Resistivity Sounding Interpretation IPI2WIN version 3.0.1. Moscow State University, Moscow.
Chiang, S., 1976. Seismic prospecting in the Ilan Plain. Mineral Technology, 215–221.
Constable, S.C., Parker, R.L., Constable, C.G., 1987. Occam's inversion: a practical algorithm for generating smooth models from electromagnetic sounding data. Geophysics 52, 289–300.
de Groot-Hedlin, C., Constable, S., 1990. Occam's inversion to generate smooth, two-dimensional models from magnetotelluric data. Geophysics 55, 1613.
Dey, A., Morrison, H., 1979. Resistivity modeling for arbitrarily shaped three-dimensional structures. Geophysics 44, 753–780.
Hsiao, P., Chiang, S., 1979. Geology and geothermal system of the Chingshui-Tuchang geothermal area, Ilan, Taiwan. Petroleum Geology of Taiwan 16, 205–213.
Hsu, S.K., Sibuet, J.C., Shyu, C.T., 1996. High-resolution detection of geologic boundaries from potential-field anomalies; an enhanced analytic signal technique. Geophysics 61, 373.
Lai, K.Y., Chen, Y.G., Wu, Y.M., Avouac, J.P., Kuo, Y.T., Wang, Y., Chang, C.H., Lin, K.C., 2009. The 2005 Ilan earthquake doublet and seismic crisis in northeastern Taiwan: evidence for dyke intrusion associated with on-land propagation of the Okinawa Trough. Geophysical Journal International 179, 678–686.
Lee, C.R., 1994. Compilation of the Geothermal Prospects Data in Taiwan During 1966–1979, 500 pp.
Lee, J.C., Angelier, J., Chu, H.T., 1997. Polyphase history and kinematics of a complex major fault zone in the northern Taiwan mountain belt: the Lishan Fault. Tectonophysics 274, 97–115.
Lin, C.W., Lin, W.H., 1995. Explanatory Text of the Geologic Map of Taiwan Sanshin, Sheet 15 Central Geological Survey. MOEA, Taiwan.
Pastana de Lugão, P., Wannamaker, P.E., 1996. Calculating the two-dimensional magnetotelluric Jacobian in finite elements using reciprocity. Geophysical Journal International 127, 806–810.
Sibuet, J.C., Deffontaines, B., Hsu, S., Thareau, N., 1998. Okinawa trough backarc basin: early tectonic and magmatic evolution. Journal of Geophysical Research 103, 30230–30245, 30267.
Sternberg, B.K., Buller, P.L., Kisabeth, J.L., Mehreteab, E., 1982. Electrical methods for hydrocarbon exploration II, Magnetotelluric (MT) method, Unconventional Methods in Exploration for Petroleum and Natural Gas. SMU Press Southern Methodist University, 202–230.
Sternberg, B.K., Washburne, J.C., Pellerin, L., 1988. Correction for the static shift in magnetotellurics using transient electromagnetic soundings. Geophysics 53, 1459–1468.
Su, F., 1978. Resistivity survey in the Chingshui prospect, I-Lan, Taiwan. Petroleum Geology of Taiwan 15, 255–264.
Tong, L.T., Ouyang, S., Guo, T.R., Lee, C.R., Hu, K.H., Lee, C.L., Wang, C.J., 2008. Insight into the geothermal structure in Chingshui, Ilan, Taiwan. Terrestrial, Atmospheric and Oceanic Sciences 19, 413–424.
Tseng, C., 1978. Geology and geothermal occurrence of the Chingshui and Tuchang districts, Ilan. Petroleum Geology of Taiwan 15, 11–23.
Wannamaker, P.E., Stodt, J.A., Rijo, L., 1987. A stable finite element solution for two-dimensional magnetotelluric modelling. Geophysical Journal of the Royal Astronomical Society 88, 277–296.